

# The melting behaviour of water and water–sodium chloride solutions studied by high-resolution Peltier-element-based adiabatic scanning calorimetry

Jan Leys<sup>1</sup> · Patricia Losada-Pérez<sup>1,2</sup> · Christ Glorieux<sup>1</sup> · Jan Thoen<sup>1</sup>

Received: 26 July 2016 / Accepted: 18 March 2017 / Published online: 8 April 2017  
© Akadémiai Kiadó, Budapest, Hungary 2017

**Abstract** Peltier-element-based adiabatic scanning calorimetry was used to obtain equilibrium enthalpy and heat capacity curves for pure water and water–NaCl mixtures, up to the eutectic mass concentration of 23.2%, in the temperature range from –30 to 5 °C, including both the eutectic and the ordinary ice melting. From these equilibrium data, information about the transition temperatures and the heats of fusion was extracted. The transition temperatures are consistent with literature data for the phase diagram. The heats of fusion were rescaled with respect to the fraction of the sample that changes phase at each transition. These rescaled values for the eutectic transition are independent of the overall salt concentration, whereas for the ice melting there is an indication of slight decrease with increasing salt concentration.

**Keywords** Adiabatic scanning calorimetry · Specific heat capacity and enthalpy · Heat of fusion · Eutectic transition · Water · Aqueous NaCl solutions

## Introduction

The energy content of a system under given circumstances is arguably the most important physical quantity defining the properties of the system. Thermodynamic descriptions

start by formulating an expression for a suitable thermodynamic potential, such as the Gibbs free energy or the Helmholtz free energy. These potentials are not directly accessible experimentally, but such formulations allow one to develop expressions which can be used to accommodate experimental data, and for sufficiently large data sets, to construct the underlying energy function.

One physical system for which such efforts have been undertaken are the aqueous solutions of NaCl, a common salt solution for which abundant experimental data are available in the literature, and for which several formulations with varying ranges of validity exist ([1–7], and references therein). Yet, to the best of our knowledge, in a specific region of the phase diagram of water–NaCl, data on thermal properties like heat capacity and transition enthalpies are sparse. For concentrations below the concentration of the water–NaCl eutectic point and at sub-zero temperatures, we could only find one relevant investigation of the heat capacity and latent heats of these solutions [8, 9]. Much of the data pertains to supercooled systems [10, 11]. The available data have generally been obtained by differential scanning calorimetry (DSC), a technique that suffers from some important intrinsic limitations that actually impede high-quality studies of phase transitions [12, 13]. These intrinsic limitations with DSC are avoided in adiabatic scanning calorimetry (ASC) developed at the end of the 1970s [14–17] and extensively used to study many different types of phase transitions and materials [12, 18–22]. However, ASCs, although further improved throughout the years, remained largely research instruments to be operated by skilled and trained personnel, not the least because of elaborate construction and complicated sample cell mounting. These handicaps have recently been eliminated in a new design of ASCs by incorporation a Peltier element between the sample cell and the adiabatic

✉ Jan Thoen  
jan.thoen@fys.kuleuven.be

<sup>1</sup> Soft Matter and Biophysics, Department of Physics and Astronomy, KU Leuven, Celestijnenlaan 200D, Box 2416, 3001 Leuven, Belgium

<sup>2</sup> Present Address: Institute for Materials Research IMO, Hasselt University, Wetenschapspark 1, 3590 Diepenbeek, Belgium

shield [13, 23, 24]. In this work, we use this novel type of Peltier-element-based adiabatic scanning calorimeter (pASC) to characterise a series of aqueous NaCl solutions in the concentration range from pure water to the eutectic NaCl concentration, covering the temperature range from just above the melting point of pure water at 0 °C to well below the crystallisation of the eutectic at −21.1 °C.

This paper is organised as follows. “[Adiabatic scanning calorimetry](#)” section gives a brief account of the adiabatic scanning calorimetric methodology and the experimental implementation of the presently used ASC. “[Measurements and results](#)” section provides basic information and discussion on the results for two samples of very pure water of different origin and on the results obtained for a series of measurements on mixtures of different composition of water and sodium chloride. “[Analysis and discussion](#)” section contains the detailed analysis and discussion of these results. In “[Summary and conclusions](#)”, section a summary and conclusions are presented.

## Adiabatic scanning calorimetry

### Measurement methodology

Adiabatic scanning calorimetry (ASC) is a calorimetric technique aimed at the simultaneous measurement of the temperature dependence of the enthalpy and the heat capacity of materials in the liquid or the solid state. The basic concept of ASC resides in applying a constant heating or cooling power to a sample holder containing the material of study. This is opposite to what is done in DSC, where a constant heating rate is imposed and the changing power needed to maintain the constant rate is measured in a differential approach with a reference sample. In ASC, the sample holder is placed in a surrounding adiabatic shield allowing one to cancel (heating mode) or to control (cooling mode) continuously the heat exchange between the sample holder and the shield during scanning with known applied constant heating or cooling power. During a run, the sample temperature  $T(t)$  is recorded as a function of time  $t$ , and the heat capacity  $C(T)$  as a function of temperature is calculated via the ratio of the known constant power  $P$  and the changing temperature rate  $\dot{T} = dT/dt$ :

$$C(T) = \frac{P}{\dot{T}}. \quad (1)$$

This leads to a continuous heat capacity curve. Moreover, the same  $T(t)$  data and the known fixed power  $P$  directly result in the enthalpy curve, since

$$H(T) - H(T_0) = \int_{T_0}^T C(T) dT = \int_{t_0}^{t(T)} P dt = P(t(T) - t_0), \quad (2)$$

where  $H(T_0)$  is the enthalpy of the system at the start time  $t_0$  of the experiment. It is a direct consequence of the constant power requirement that the integral can be simply solved.

The main advantage of ASC is the potential to obtain high-resolution equilibrium enthalpy and heat capacity data. Because the sample is given a fixed amount of energy per unit of time, which it can use “as it wants”, to heat up or change its phase, the sample is effectively in control of the calorimeter. In other words: the calorimeter follows the behaviour of the sample. This feature, combined with the slow scanning rates that can be achieved, allows studying the sample in nearly ideal thermal and thermodynamic equilibrium conditions. As more extensively discussed elsewhere, this cannot be achieved by the common DSC instruments [12, 13].

### Experimental

An essential requirement for a high-resolution adiabatic scanning calorimeter operating in the heating mode is the equality (mK or better) of the temperatures of the adiabatic shield and of the sample (holder) in weak thermal contact with this surrounding adiabatic shield. For operations in the cooling mode, a constant preset temperature difference between the sample and the shield has to be maintained within the same temperature stability limits. The “classical” ASC implementations used elaborate construction and calibration procedures to achieve these conditions [17, 21]. All this made these ASC instruments complicated, and they needed to be operated by a skilled and well-trained person.

In the present type of ASC [13, 23–26], used for the results presented here, these problems are completely eliminated by inserting a very sensitive (of the order of 10 mV K<sup>−1</sup>) semiconductor-materials-based Peltier element (PE) as temperature difference detector between the sample and the shield. The μK sensitivity of the PE for temperature differences allows, in combination with a proper servo-system, to maintain almost perfect equality of the sample and shield temperatures in the heating mode. For the cooling mode, a preset temperature difference between sample and shield can be kept constant with equal resolution. Details on the construction of the pASC implementation of the ASC concept can be found elsewhere [13, 24, 26]. With the pASC used for the present investigation, the uncertainty on the absolute values of specific heat capacity and enthalpy is about 2%, while the

resolution in these quantities and in the measured temperatures is much higher.

## Measurements and results

### Materials and samples

For the measurements on pure water and for the preparation of the different mixtures, we used HPLC grade water (code W/0106/17, batch 0625273) purchased from Fisher Scientific. Sodium chloride was purchased from Aldrich (Product Number 204439, lot MKBH4096V, nominal purity 99.999%). In addition to the HPLC grade water sample, we also measured a sample that was taken from a one litre bottle of commercially available natural mineral water (SPA Reine, Spa Monopole, Belgium). Mixtures were prepared in quantities of typically several cm<sup>3</sup> of which 30–80 mg was then transferred into stainless steel sample holders (Mettler-Toledo 120  $\mu$ L medium pressure DSC crucible) and subsequently hermetically sealed.

### Investigated part of the phase diagram of water–NaCl

In comparison with the phase diagram of a one-component system (exhibiting transitions between solid, liquid and gas), the phase diagram of mixtures with two or more components can be quite complicated and exhibit new phenomena when heated or cooled or when their composition is changed. In a two-component system, which is the case here, phase separation in the liquid and/or solid phases is quite common. Of particular interest here is a liquid–solid phase diagram with an eutectic point [28, 29]. Such a point has a specific composition, and the mixture melts at a fixed temperature directly from the solid phase to a homogeneous liquid solution. In mixtures of water and NaCl, such a eutectic point has mass fraction  $x_{\text{eut}} = 23.2\%$  and a melting temperature of  $T_{\text{eut}} = -21.1\%$  (see the phase diagram of Fig. 1). For mixtures with lower NaCl concentrations, the transition from the homogeneous liquid solution (above the solid blue line in Fig. 1a) is more complicated. In cooling a solution from high temperatures, it is observed that the solution stays liquid for temperatures below the melting temperature of pure water (often called melting point depression). In further decreasing the temperature, solid ice is gradually formed in the solution. Since this reduces the liquid water content in the solution, it becomes more and more salty. This reduction of the amount of water in the liquid solution goes on until at the eutectic temperature its composition reaches that of the eutectic point and the system transfers into a solid mixture

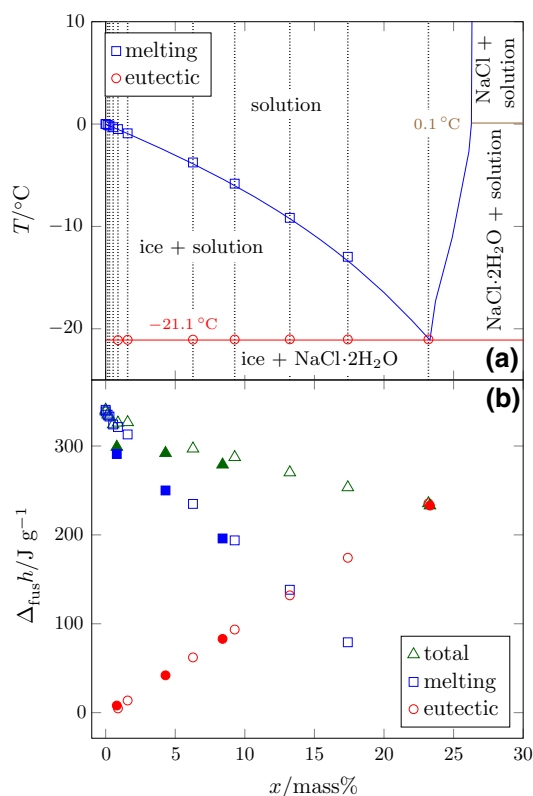


**Fig. 1** **a** The phase diagram of water–NaCl for low salt concentrations. The blue, red and brown solid lines indicate the limits of the various two-phase regions [27]. The vertical black dotted lines correspond to the concentrations of the samples studied in this work. The symbols indicate the transition temperatures as determined in this work. **b** Transition enthalpies for the eutectic and melting processes, from this work (open symbols) and Han et al. [9] (closed symbols). (Color figure online)

of ice and salt hydrate. In this investigation, we explored the part of the phase diagram of mixtures of water and sodium chloride for  $x \leq x_{\text{eut}}$ . Table 1 gives an overview of the different samples that have been measured. Figure 1 shows their position in the water–NaCl phase diagram [27].

### Results for the pure HPLC water sample and for the natural mineral water sample

When pure solidified water, Sample 1, is provided with a constant power, it heats up according to the temperature profile in Fig. 2a. Starting as ice at  $-15\text{ }^\circ\text{C}$ , the temperature increases nearly linearly until it remains constant at  $0\text{ }^\circ\text{C}$ . The provided power is then used for the conversion of ice to water, and only after all ice has melted, the temperature starts to rise again. Equation (2), with  $H(T_0) = H(-15\text{ }^\circ\text{C}) = 0$ , can immediately be used to evaluate the specific enthalpy  $h$  of the sample. This is displayed in Fig. 2b. It is also indicated how a first estimate for the enthalpy of the transition  $\Delta_{\text{fus}}h$  can be obtained on the basis of these data. In Fig. 3a, the  $h(t)$  data are replotted as  $h(T)$ , and the phase transition becomes

**Table 1** Overview of the different samples and results for transition temperatures and enthalpies

#	Name	$x/\text{Mass}\%$	$x_m/\text{mol}\%$	$m/\text{mg}$	$f_{\text{eut}}$	$f_w$	Eutectic			Melting		
							$T_{\text{tr}}/\text{°C}$	$\Delta_{\text{fus}}h/\text{J g}^{-1}$	$\Delta_{\text{fus}}h_{\text{scaled}}/\text{J g}^{-1}$	$T_{\text{tr}}/\text{°C}$	$\Delta_{\text{fus}}h/\text{J g}^{-1}$	$\Delta_{\text{fus}}h_{\text{scaled}}/\text{J g}^{-1}$
1	Fisher	0	0	57.3	0	1				0.005	340.7	
2	Spa	0	0	46.5	0	1				0.005	338.9	
3		0.1388	0.04283	38.9	0.0060	0.9940				-0.078	335.3	
4		0.2733	0.08439	42.3	0.0118	0.9882				-0.150	333.2	
5		0.5381	0.1665	29.8	0.0232	0.9768				-0.311	324.2	
6		0.8831	0.2739	43.3	0.0381	0.9619	-21.110	4.8	126.1	-0.491	321.4	334.1
7		1.579	0.4920	34.6	0.0681	0.9319	-21.080	13.7	200.9	-0.905	313.0	335.9
8		6.273	2.021	37.2	0.2704	0.7296	-21.061	62.1	229.8	-3.754	234.9	321.9
9		9.271	3.054	67.5	0.3996	0.6004	-21.050	93.5	234.0	-5.823	193.8	322.9
10		13.232	4.490	71.7	0.5703	0.4297	-21.030	131.9	231.4	-9.163	138.3	321.8
11		17.400	6.098	83.3	0.7500	0.2500	-21.042	174.2	232.3	-12.968	79.2	316.8
12	Eutectic	23.193	8.516	76.6	0.9997	0.0003	-21.035	235.5	235.6			

The transition temperatures are obtained from the intersection of the extrapolations of the  $h(T)$  data in the upper transition region and the higher-temperature phase. The transition enthalpies have been obtained following the procedure of “[Calculation of the molten fraction](#)” section. For the rescaling according to the lever rule, the eutectic and ice fractions  $f_{\text{eut}}$  and  $f_w$  have been calculated with respect to the literature eutectic concentration of 23.2%

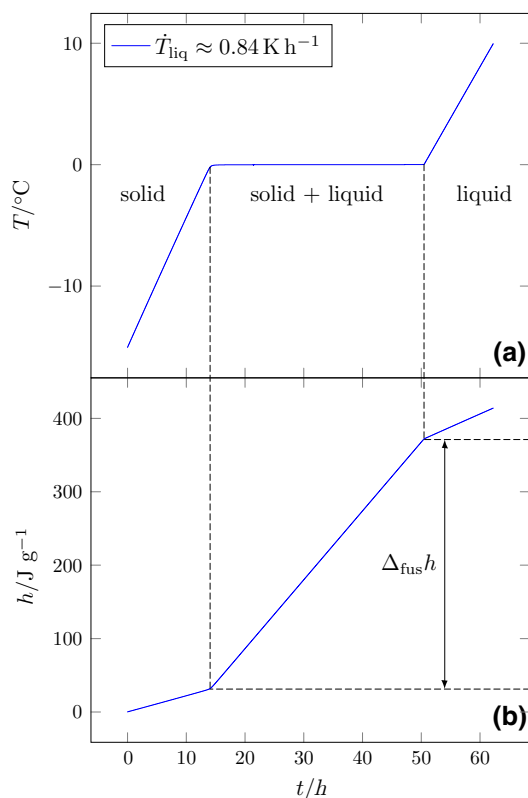


**Fig. 2** pASC results for Sample 1 of pure (Fisher) water. **a**  $T(t)$ , showing the temperature increase in the solid and liquid phases and the constant temperature during phase conversion at 0°C. **b**  $h(t)$ , indicating how the transition enthalpy  $\Delta_{\text{fus}}h$  can be extracted

now visible as an essentially vertical step in the enthalpy at 0°C. The height of this step, as indicated in the figure, corresponds to the transition enthalpy  $\Delta_{\text{fus}}h$ .

If now Eq. (1) is used, the specific heat capacity can be calculated, which is presented in Fig. 3b. The heat capacity shows most clearly the advantages of pASC. The small average scanning rate and equilibrium operation lead to a very sharp peak, which is only broadened by impurity effects (as we will discuss below). In marked contrast with DSC results is the sharp end of the peak, as instrument-related broadening is absent in pASC. The data are greatly truncated: the highest value of  $c_p$  attained here is of the order of  $10^6 \text{ J g}^{-1} \text{ K}^{-1}$ , where it should be stressed that the recorded  $c_p$  during the transition is only an effective value. For a perfectly pure system, the melting would take place at a single temperature, leading to a perfect step in  $h(T)$  or equivalently to  $\dot{T} = 0$ . Using either  $c_p = (\partial h / \partial T)_p$  or Eq. (1), one sees that  $c_p = \infty$  at this idealised transition. Thus, the height and sharpness of the peak are also a purity measure.

Spa mineral water (Sample 2), as can be asserted from its taste, is not a salt solution, although by its nature as natural spring water, some impurities should be present. Hence, a somewhat broadened melting transition is expected in comparison with the Fisher HPLC water. However, comparison of  $h(T)$  and  $c_p(T)$  between these two samples in Fig. 4 shows that the curves are hardly distinguishable. To get a better idea of the scale of the difference, the curves for the most dilute salt solution, Sample 3

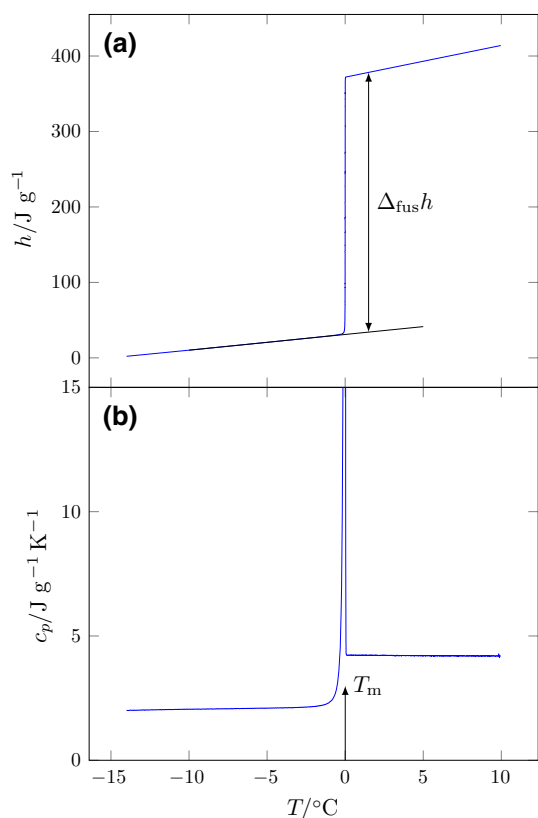


**Fig. 3** pASC results for Sample 1 of pure (Fisher) water. **a**  $h(T)$ , indicating how the transition enthalpy can be extracted as the height of the step. **b**  $c_p(T)$ , indicating the transition temperature and showing the sharpness of the transition peak

of 0.139%, are also included. On the basis of this figure, one can conclude that Spa is nearly as pure as Fisher water. In any case, it contains much less than 0.139% of impurities. We will quantify and discuss the purity of these sample in “Purity determination for the water samples” section.

### Results for the water–sodium chloride mixtures

The eutectic transition in water–NaCl solutions is very susceptible to supercooling, and therefore, these samples were cooled to  $-33\text{ }^{\circ}\text{C}$  for the three lowest concentrations and  $-50\text{ }^{\circ}\text{C}$  for the higher concentrations and left overnight before the actual heating experiments were started. For the lower concentrations, Samples 3, 4 and 5, it turned out that even a prolonged stay at  $-33\text{ }^{\circ}\text{C}$  is insufficient to crystallise. This is not highly relevant for our analysis, because the corresponding eutectic peaks are very small.

Figure 5 shows  $c_p(T)$  for selected concentrations. From these data, the main effects of increasing the salt concentration can be observed. The first and most obvious one is the presence of an extra peak at  $-21.1\text{ }^{\circ}\text{C}$ , which corresponds to the disappearance of the  $\text{NaCl}\cdot 2\text{H}_2\text{O}$  solid. The

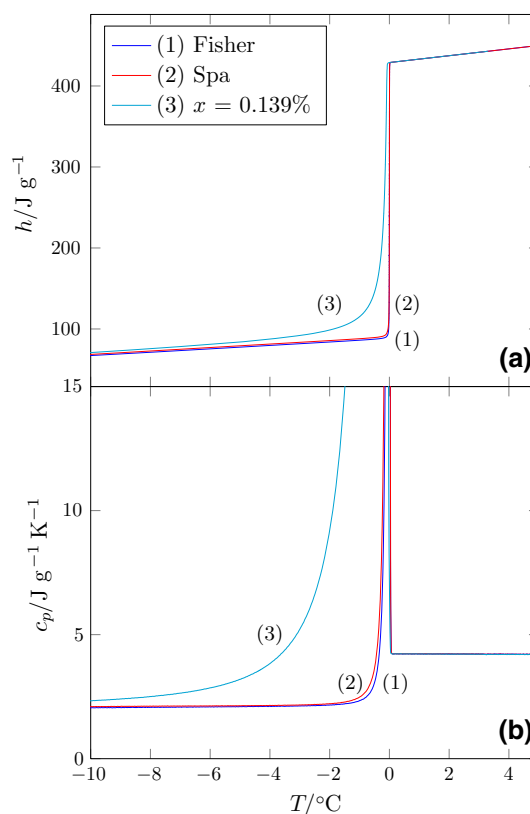


**Fig. 4** A comparison of Fisher and Spa water (Samples 1 and 2), complemented with the most dilute salt solution (Sample 3). **a**  $h(T)$ , normalised to  $450\text{ J g}^{-1}$  at  $5\text{ }^{\circ}\text{C}$  for a clear presentation. **b**  $c_p(T)$ . Both curves clearly indicate that the purity of Spa mineral water, as seen from thermal data, is very close to that of the Fisher HPLC water

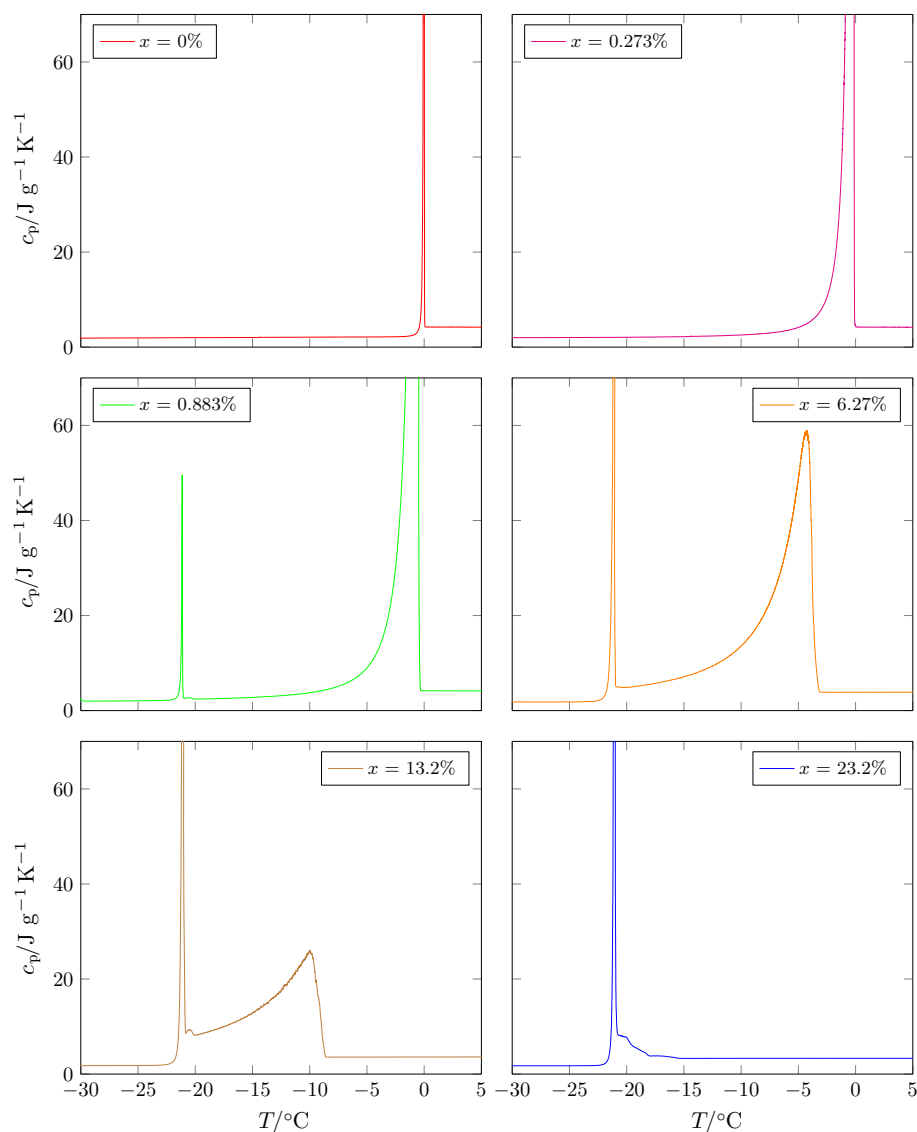
eutectic transition temperature does not depend on the salt concentration, but the peak becomes more prominent with increasing concentration, although it remains equally sharp for all samples. The second observation is the broadening of the ice melting peak: already quite clear for  $x = 0.8333\%$ , the peak fills the entire range down to the eutectic peak for  $x = 6.27\%$ . This broadening is accompanied by a decrease of height. Finally, the temperature of the melting peak decreases systematically with concentration.

The curve for the eutectic composition, 23.2%, shows some small bumps between the eutectic peak and  $-15\%$ . These indicate that we are very close to, but not exactly at the eutectic concentration. Given the high sensitivity of pASC, the deviation may be very small, and we treat this concentration further on as the eutectic one.

### Comparison to the literature data

The absolute values of  $c_p$  of the solutions in the liquid region agree well with the data from Ref. [11]. Our determination of the transition heat of water,

**Fig. 5** Specific heat capacity  $c_p(T)$  of selected water–NaCl solutions (Samples 2, 4, 6, 8, 10 and 12), showing the effects of increasing salt concentration: broadening of the melting transition peak, decreasing melting temperature and emergence of the eutectic peak, as well as the increasing importance of the latter at the expense of the melting peak



$(340 \pm 7) \text{ J g}^{-1}$ , is a bit larger than the standard value  $333 \text{ J g}^{-1}$  [30], but this lies within the current limits of uncertainty that are established for our calorimeter.

For pure water, Sample 1, the heat capacity curve is compared in Fig. 6 with the curve obtained by Inaba et al. [31] who constructed a particularly sensitive DSC instrument, capable of measuring at low scanning rates. Their results were reported as heat flow data and were converted here to  $c_p(T)$  data for inclusion in Fig. 6. This DSC used a rate of  $3.6 \text{ K h}^{-1}$ , the same order of magnitude as the ASC run away from the transition. Yet, it is clear that the use of a constant rate, even a low one, in DSC broadens the phase transition, and shifts it to higher temperatures, even if the temperature where the transition becomes noticeable in the  $c_p(T)$  curves is about the same in both calorimeters.

Also for the salt solutions, some DSC heat flow curves have been published. In particular, we refer to the DSC heat flow curves that are published in Ref. [9], where a selection of water–NaCl solutions in the same concentration range were studied. The DSC curves show the same tendencies as we see here, but with a much reduced resolution. The eutectic peaks appear much broader in that work, the melting peaks are stretched out to higher temperatures. No observations can be made concerning the behaviour between the peaks as a consequence of the used scale. The shape of the eutectic peak as seen in DSC may be better asserted from Ref. [32], where it is presented as heat flow data for a  $0.154 \text{ M} = 0.9\%$  solution, a composition close to our Sample 6. The peak is sharper than for the Han et al. data, while it also displays the high-temperature shoulder that appears in the ASC data. Another example of

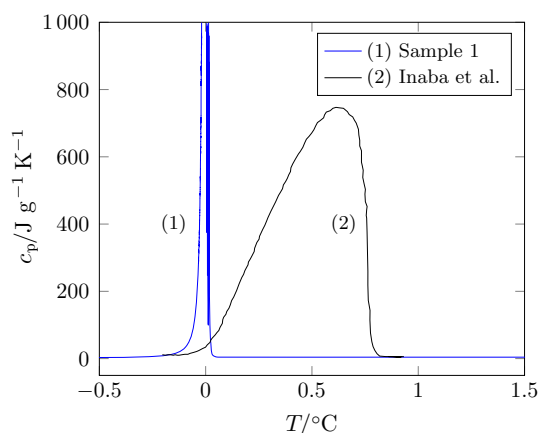


**Fig. 6** Comparison of  $c_p(T)$  near the melting point of water, obtained with pASC from Sample 1, pure water and as measured by custom-built high-resolution DSC at a comparable temperature scanning rate [31]

a DSC result is given in Ref. [8]. However, the presented curve concerned a salt solution that contained also compounds other than the dominant NaCl. In this example, the eutectic peak with an onset at about  $-26^\circ\text{C}$  is much broader than in the earlier DSC data as well as in the ASC data. Nevertheless, the basic shape of  $c_p(T)$  data for Sample 9, which has a similar concentration, is comparable to this heat flow data.

### Enthalpy curves

An overview of the observations that we have made so far can be achieved by the plot of  $h(T)$  for all samples in Fig. 7. In this figure, the enthalpy has been normalised to  $450\text{ J g}^{-1}$  at  $5^\circ\text{C}$ ; such a shift corresponds to an appropriate choice of  $H_0$  in Eq. (2). Equating the  $h(T)$  values in the liquid phase leads to a clear view of the energetic situation in the solid phase and the two-phase region. It can immediately be verified that the eutectic transition always takes place at  $-21.1^\circ\text{C}$ , and is sharp regardless of the overall concentration. In contrast, the end temperature of the ice melting decreases and the transition becomes very broad, finally disappearing for the eutectic concentration. The eutectic transition enthalpy increases, whereas the enthalpy of the ice melting decreases.

An observation that is not simple to make on the basis of  $c_p(T)$  is now trivially possible. With increasing salt concentration, the total amount of heat needed to melt from the ice +  $\text{NaCl}\cdot 2\text{H}_2\text{O}$  fully solid mixture at for example  $-28^\circ\text{C}$  to the liquid decreases considerably. This observation is valid for the range between  $-28$  to  $5^\circ\text{C}$ , as well as the range between  $-28^\circ\text{C}$  and the end of the ice melting transition, as shown in Fig. 8. This effect scales essentially linearly with the overall concentration of the salt, both with

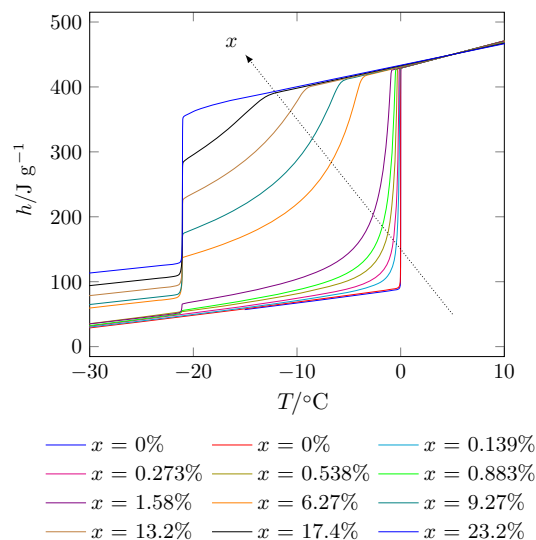


**Fig. 7** Overview of the enthalpy for all the water–NaCl samples, showing the important features of the samples with increasing salt concentration. The eutectic transition temperature is constant at  $-21.1^\circ\text{C}$  and the melting temperature decreases. The transition enthalpy of the eutectic transition increases at the expense of the melting enthalpy. Also, the melting transition becomes broader

the mass concentration as depicted in Fig. 8, as with the molar concentration.

## Analysis and discussion

### Calculation of the molten fraction

The unique possibility of ASC, yielding simultaneously thermodynamic equilibrium data for the enthalpy and heat capacity during the whole melting process of a sample, allows for an alternative approach for the determination of the heat of fusion (latent heat) and for extracting the mole fraction of the solute from those data, at least in the case of ideal solutions. Both of these require the same underlying calculation, namely the determination of the molten fraction  $F$ , which quantifies the fraction of the sample that has transitioned from the low-temperature phase to the high-temperature phase.

Since at a melting transition,  $\Delta_{\text{fus}}h$  represents the total energy that is needed to go from one phase to the other, a natural way of determining the molten fraction is comparing the energy provided for the melting of the sample up to a temperature  $T$  with  $\Delta_{\text{fus}}h$ :

$$F(T) = \frac{h'(T)}{\Delta_{\text{fus}}h}. \quad (3)$$

In this equation,  $h'(T)$  denotes the measured enthalpy increase related to melting up to temperature  $T$  and  $\Delta_{\text{fus}}h$  the measured total enthalpy increase over the transition, the

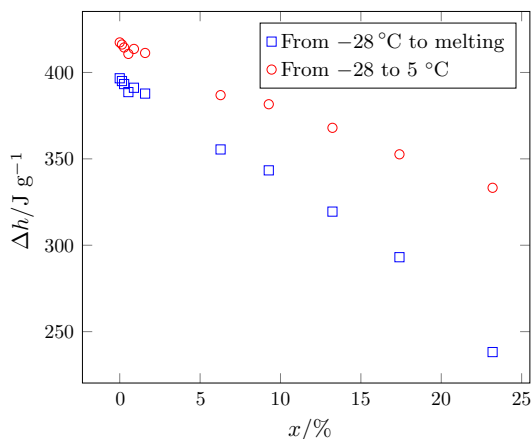


**Fig. 8** Enthalpy increments per g of sample between  $-28\text{ }^{\circ}\text{C}$  and either the end of the ice melting or  $5\text{ }^{\circ}\text{C}$ . These represent the energy needed to heat the entire sample over the respective temperature ranges

latent heat.  $h'(T)$  only refers to the enthalpy change related to the melting process, and it does *not* include the heat that is needed to increase the sample temperature during melting. This latter heat is present, and the melting is not fully isothermal because the transition is broadened due to the presence of impurities. Therefore, some heating is needed to achieve the higher temperature on which the sample can continue to melt.<sup>1</sup> Thus, in determining  $h'(T)$ ,  $\Delta_{\text{fus}}h$  and consequently  $F$  of Eq. (3), one should realise that these quantities relate only to the changes induced by the melting process. In the two-phase region, the energy needed to heat the liquid part and solid part has to be subtracted from the measured total enthalpy. This is particularly relevant if the specific heat capacity of the solid and the liquid are quite different, or if the transition is relatively broad.

In DSC, this subtraction is usually done by subtraction of an ad hoc choice of different types of heat capacity baselines, for example linear interpolations or different types of sigmoidal baselines. The fact that in ASC thermal and thermodynamic equilibrium data are obtained in the solid and liquid phase and over the entire two-phase region allows for a more rigorous approach [13, 24].

The procedure starts by defining the heat capacity of the lower- and higher-temperature phases (which we will call here solid and liquid) far away from the transition, where they can be considered as uninfluenced by the phase transition. In such a linear region of  $c_p(T)$  below the transition, the data of the solid phase are fitted by a straight line. The same is done for the liquid phase above the transition, resulting in

<sup>1</sup> For an ideal, impurity-free sample, the enthalpy would make a step at the melting temperature  $T_{\text{tr}}$  of the exact value of  $\Delta_{\text{fus}}h$ , and  $F(T)$  would become a step function that is 0 below  $T_{\text{tr}}$  and 1 above.

$$c_s = A_s + B_s T \quad (4)$$

$$c_l = A_l + B_l T. \quad (5)$$

In the melting region, the heat capacity baseline  $c_{\text{sl}}(T)$ , which is composed of the added heat capacities of the solid and liquid fractions of the sample, can be written as

$$c_{\text{sl}}(T) = c_l(T)F(T) + c_s(T)[1 - F(T)]. \quad (6)$$

For a given (estimate of)  $F(T)$ , the quantity  $h'(T)$  can now be calculated via

$$h'(T) = h(T) - \int_{T_b}^T c_{\text{sl}}(T) dT, \quad (7)$$

where  $T_b$  is the starting temperature of the phase transition region. It is obvious that the above system of equations that defines  $F(T)$  cannot easily be solved, and therefore, an iterative approach is used. A zero-order approximation  $F_0(T)$ , with  $F_0(T) = 0$  below a certain temperature  $T_s > T_{\text{tr}}$  and  $F_0(T) = 1$  above  $T_s$ , is inserted in Eq. (6). Then,  $h'_0(T)$  can be calculated through Eq. (7), from which a first estimate  $\Delta_{\text{fus}}h_0$  can be found, and this gives then the first iterated value  $F_1(T)$  with Eq. (3). This  $F_1(T)$  then serves as the starting point for the next iteration, and the procedure can continue until the desired accuracy is achieved. In Fig. 9, some iterative  $F_i$  results between  $i = 0$  to  $i = 4$  are given for Sample 4 (0.273%). This number of four iterations has proven to be sufficient for any sample.

The method as described above is applied to Sample 1 and 2 in this work, but for the salt solutions, there is a complication. Above the eutectic transition temperature, the concentration of the liquid part of the system cannot be considered constant: as more pure ice melts, the solution becomes more dilute, until at the end of the ice melting temperature the nominal concentration is reached. As the heat capacity of salt solutions increases with decreasing concentration, a linear extrapolation of the liquid heat capacity as used in Eq. (5) would lead to a systematic overestimation of the background heat capacity  $c_{\text{sl}}$  and consequently an underestimation of  $\Delta_{\text{fus}}h$ . Therefore, the procedure above was slightly modified to replace  $c_l$  with the interpolated literature heat capacity data for the supercooled salt solutions [11]. This modification changed the values  $\Delta_{\text{fus}}h$  by at most 1%, the difference being the most pronounced for the samples between 6 and 13%, where the broadening of the transitions is large, as well as the temperature range of the two-phase region.

### Transition temperatures

For determining transition temperatures on the basis of DSC  $c_p(T)$  data, two methods are commonly used. The simplest of these uses the temperature of maximum  $c_p$  as



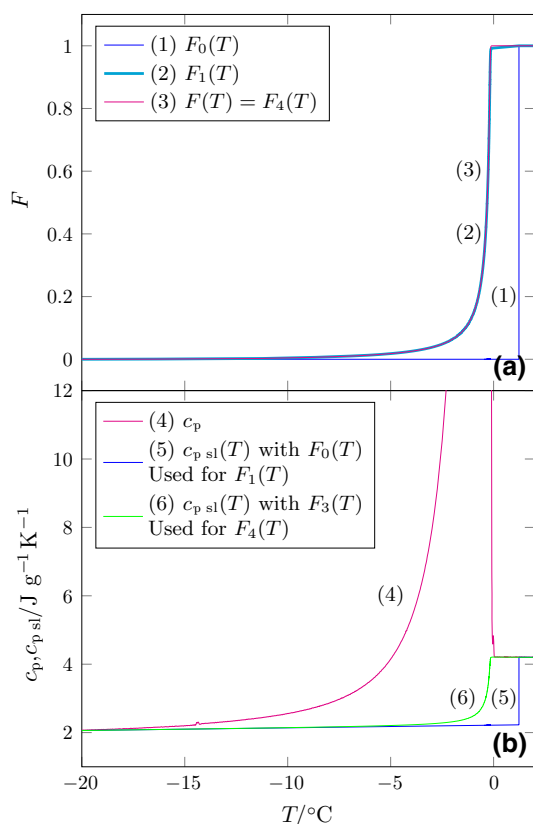


**Fig. 9** Illustration of the iterative calculation of  $F(T)$  for Sample 4 of 0.273%. **a** The molten fraction  $F(T)$  and selected intermediate steps for the iteration procedure. The final  $F(T)$  result mostly obscures the curve from the initial iteration. **b** Specific ( $c_p$ ) and background specific heat capacity ( $c_{sl}$ ) for intermediate steps

$T_{tr}$ . The second method uses the onset temperature, defined as the intersection between an extrapolation of the solid  $c_p$  and a linear fit to part of the transition peak [33]. There are arguments against the first method. It fails to incorporate the rate dependence in DSC, and  $T_{tr}$  will depend on the rate. This can eventually be overcome by an extrapolation of  $T_{tr}$  from multiple rates to zero-rate. Also, it is not clear whether the maximum of the peak has any physical meaning due to the important influence of the instrument on the result. For the second method, the rate dependence is partly overcome: because this definition relates to the temperature where the sample first clearly starts to melt (in the view of the DSC method), it is intrinsically less dependent on the rate. But, it may be strongly dependent on the interpretation of the operator and, more importantly, on the properties of the transition. For the higher concentration samples, the melting phase transition is very broad, and the  $c_p$  curve strongly curved. This makes it unclear how to choose the extrapolation lines, especially the one corresponding to the slope of the peak. Finally, one may ask whether it would not make more sense to consider the end

of the phase transition. In many cases, this side is thermodynamically much sharper defined in enthalpy and heat capacity, not influenced by multiple possible pre-melting effects in the more ordered phase. This sharpness is very clear in our ASC data. These observations lead naturally to the choice of the end of the melting temperature as the transition temperature  $T_{tr}$ .

These considerations have led us to investigate several methods for the determination of the transition temperatures. For all methods, we take the end of the transition as the defining point. Since ASC obtains equilibrium data, it is more sensible to discuss the temperature where the transition is completed, rather than, like in DSC, focus on the region where the transition becomes detectable in out-of-equilibrium data.

It is possible to read  $T_{tr}$  from the  $c_p(T)$  curves as the temperature where the  $c_p$  transition peaks ends, this is for most transitions a nearly  $90^\circ$  angle. Another approach can be based on the values of  $F(T)$ . Since the transition is, by definition, finished when  $F$  reaches 1, we can define the transition temperature this way. In practice, however, we have used  $T(F = 0.99)$  as the transition temperature, in order to avoid any numerical difficulties that may arise by choosing the limit at exactly 1. For most practical cases we have encountered, this approach led to a value that would correspond within 10 mK to the temperature that according to a visual assertion of the  $F(T)$  would correspond to  $T(F = 1)$ . For these two methods, the results largely agree with each other, and also with the third method that will be introduced below.

This third method bears some similarity to the onset temperature method from DSC, but then applied to  $h(T)$  data.  $T_{tr}$  is taken as the temperature where two lines intersect: a linear extrapolation of  $h(T)$  in the higher-temperature phase just above the phase transition, and a linear extrapolation of  $h(T)$  in that part of the transition where it can be reasonably well described by a linear approximation. This latter definition seems arbitrarily, but in most cases, it corresponds to the upper half of the enthalpy in the transition region for the eutectic and to the upper quart for the ice melting. This contrasts with the onset temperature determination in DSC, which is focussed on the lower parts of the transition peak. In Table 1, the results for the melting and the eutectic peak are summarised, and they are compared with the literature phase diagram in Fig. 1a.

### Transition enthalpies

As explained in “Calculation of the molten fraction” section, the calculation of  $F(T)$  on the basis of  $h(T)$ ,  $c_p(T)$  and the derived  $c_{sl}$ , also leads to values for  $\Delta_{fus}h$ . In our earlier work [13, 24], as well as for the low-concentration samples

in this work, we found that this method gives good results for relatively sharp transitions. But for samples with higher concentration, the presence of two transition peaks in the solutions, together with the broadening of the ice melting range, makes this approach unsuitable. In particular, the determination of the extrapolations  $c_s$  and  $c_l$  for Eqs. (4) and (5) becomes ambiguous.

Thus, we apply the method to the entire region and not to each of the transitions separately. This means that  $c_s$  is obtained from ice + NaCl·2H<sub>2</sub>O below about  $-23^\circ\text{C}$ , whereas  $c_l$  is obtained from the fully liquid solution above the melting point.

However, the obtained  $\Delta_{\text{fus}}h$  would correspond to the melting enthalpy for the two combined transitions, and we need a means to split this into the eutectic and the ice melting contribution. From its definition in “[Calculation of the molten fraction](#)” section, it can be seen that  $h'(T)$  will be equal to 0 below a given transition and equal to  $\Delta_{\text{fus}}h$  above that transition, as illustrated in Fig. 10 for Sample 8. By selecting appropriate limiting temperatures for the parts of  $h'(T)$  corresponding to the eutectic transition and to the ice melting transition, a  $\Delta_{\text{fus}}h$  can be associated to each of these transitions. The  $\Delta_{\text{fus}}h$  values obtained this way are reported in Table 1. For the low-concentration samples, we compared the value for  $\Delta_{\text{fus}}h$  for the melting obtained from this approach to  $h'(T)$  with the results from the direct calculation as outlined in “[Calculation of the molten fraction](#)” section, and the values are essentially identical.

### Concentration dependence of the transition enthalpy

In the previous section, we have reported the  $\Delta_{\text{fus}}h$  values with respect to the mass of the total sample. But, as the phase diagram in Fig. 1 indicates, once below the start of the ice freezing temperature of the solution, there are in

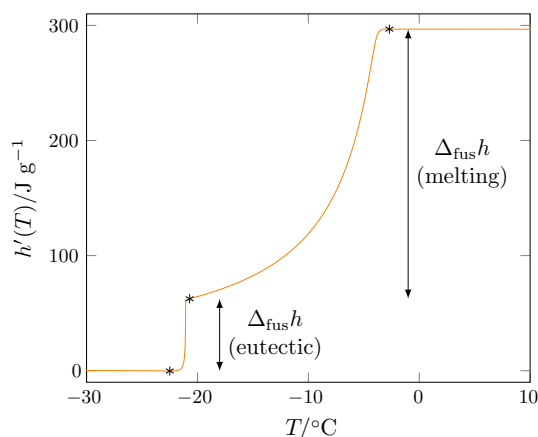


**Fig. 10**  $h'(T)$  for Sample 8, as used for the determination of  $\Delta_{\text{fus}}h$  for the melting. The three stars near  $-23$ ,  $-21$  and  $-3^\circ\text{C}$  indicate the limits of the transition regions

fact two distinct phases in the system, a solid (ice) and a liquid (salt solution) one. Pure water gradually freezes out of the solution, and the remaining fraction of the solution is a salt solution of increasing salt concentration. Upon further cooling below  $-21.1^\circ\text{C}$ , also this fraction crystallises at the eutectic temperature. Therefore, in the temperature range between the upper limit of the ice melting and the eutectic temperature, the variation in the initial NaCl concentration of the solution is reflected by the presence of different amounts of pure water ice and aqueous salt solution. These amounts can be obtained from the phase diagram by applying the lever rule [34]. This also means that upon heating the total amount of transition enthalpy can be considered as the result of two separate processes. Starting at sufficiently low temperature, there is first the melting of ice + solid salt hydrate and the dissociation of the NaCl·2H<sub>2</sub>O [always at  $-21.1^\circ\text{C}$  and with transition heat  $\Delta_{\text{fus}}h(\text{eutectic})$ ]. This leads to a system with a salt solution of the eutectic composition and solid pure ice in fractions corresponding with the overall composition in the fully liquid phase. Upon further temperature increase, the ice gradually melts and the liquid solution dilutes up to a maximum temperature ( $T_{\text{tr}}$  of melting in Table 1). With this pure ice melting, the corresponding transition heat  $\Delta_{\text{fus}}h(\text{melting})$  is associated. This separation in two distinct processes might possibly imply that the total melting in  $\text{J g}^{-1}$  with respect to the total mass of the sample can be rescaled to the masses of the melting fractions of the sample involved in the separate transitions.

This procedure has been performed earlier for aqueous NaCl solutions [8, 9]. These authors reported that the melting of the pure water ice fraction in the solutions requires  $303.7 \pm 2.5 \text{ J g}^{-1}$ , while the melting of the eutectic fraction requires  $233.0 \pm 1.6 \text{ J g}^{-1}$ , both independent of salt concentration. They also remarked that the former value for water/ice deviates substantially from the literature value for pure water,  $333 \text{ J g}^{-1}$  at  $0^\circ\text{C}$ , for reasons that are not clear. On the other hand, the value for the eutectic fraction was the same as obtained from their measurement of the eutectic concentration. We have repeated this analysis on the basis of our ASC results, and the outcome is summarised in Table 1 and Fig. 1b.

For the eutectic fraction, the values for the scaled  $\Delta_{\text{fus}}h$  are corresponding closely to the measured value for the eutectic concentration, both in this work and from the earlier work of Han et al. This can be expected: the eutectic transition is rather narrow, even in a DSC run, and hence, problems related to the background determination will be minimal in either technique. Exceptions are Sample 6 and to some extent Sample 7, with quite small eutectic peaks. Since these peaks are very small, the uncertainty is quite high here and some supercooling of the eutectic transition

might also be present for Sample 6 that was only precooled to  $-33\text{ }^\circ\text{C}$ .

For the melting of the pure water fraction, the values are close to  $\Delta_{\text{fus}}h$  of pure water, with a small tendency to decrease for the higher concentrations. Thus, our results clearly disagree with those of Han et al. We find values that are larger than the  $303.7\text{ }^\circ\text{C}$  these authors reported. In order to attempt to understand this difference, we first note that, on the above separation of the transitions, a value corresponding to  $\Delta_{\text{fus}}h$  of pure water should be expected. The ASC results adhere within 5% for all concentrations except the highest one. For this concentration, the smallness of the peak and closeness to the eutectic one might be at the origin of the deviating value. However, the correspondence decreases a bit with increasing concentration. As a first reason for this decrease and the deviation observed by Han et al., one might think at uncertainties in the determination of background, which is intrinsically more difficult in DSC. However, the possibility of the effect of temperature dependence of  $\Delta_{\text{fus}}h$  by the melting point depression should not be ignored [35].

**Purity determination for the water samples**

Thermal data can be used to determine the purity of the samples. The method to achieve this is well established [36–38] and often used in combination with DSC experiments [39–44]. However, the method is subject to stringent assumptions about the ideality of a system [34]. Assuming that only the number of impurity “particles” plays a role (colligative property), the mixing of the pure compound and the impurity is ideal, and the impurity is only present in the liquid part of the sample, the van ’t Hoff relation can be derived [45]. We have modified this method for use with ASC data, a discussion can be found in Refs. [13, 24].

Unfortunately, it is well established for the uni-univalent electrolyte NaCl in water that activity coefficients deviate substantially from the ideal value of one even for very dilute solutions [46]. This makes the van t Hoff equation not applicable for these NaCl salt solutions. Since the impurities in the two “pure” water samples are not known and the impurity level expected to be very low, the van t Hoff approach should be applicable.

Usually, not the full form of the derived equation is used, but instead, a linearisation is made, assuming a small concentration of impurities, leading to

$$T = T_0 - \frac{RT_0^2}{M_w \Delta_{\text{fus}}h} x_2 \frac{1}{F} \tag{8}$$

Here  $T_0$  is the melting temperature of the pure compound,  $R$  the gas constant,  $M_w$  the molar mass of the pure compound,  $\Delta_{\text{fus}}h$  the phase transition enthalpy,  $x_2$  the molar concentration of the impurities and  $F$  the molten fraction.

Equation (8) suggests a linear relation between  $T$  and  $1/F$ , but in real systems this is almost never observed. One way to resolve this is to linearise the data, a procedure described in an ASTM standard [47] and often used in the literature [41, 42, 44], sometimes with small variations [38]. The linearisation is performed by, in the notation of this paper, replacing  $F$  by

$$F_\epsilon(T) = \frac{h'(T) + \epsilon}{\Delta_{\text{fus}}h + \epsilon}, \tag{9}$$

where  $\epsilon$  is a correction factor, required to be smaller than 20% of  $\Delta_{\text{fus}}h$  [47]. It is also common to find  $F_\epsilon$  defined without  $\epsilon$  in the numerator.

Mastrangelo and Dornthe eliminated one assumption from the derivation of the van ’t Hoff relation. In their model, the impurity could be present in the solid part of the sample [40, 48]. They arrived at

$$T = T_0 - \frac{RT_0^2}{M_w \Delta_{\text{fus}}h} x_2 \frac{1}{F + \frac{K}{1-K}}, \tag{10}$$

where  $K$  is the ratio of the amount of impurity in the solid phase to that in the liquid phase.  $T_0$ ,  $x_2$  and  $K$  can be obtained by reading out  $T$  from the  $T(F^{-1})$  curve at  $F = 0.25$ ,  $F = 0.5$  and  $F = 1$ , inserting these values in Eq. (10) and solving the resulting set of equations. In our analysis, we rescaled these points to  $F = 0.1$ ,  $F = 0.3$  and  $F = 0.5$  and adapted the calculation appropriately; this also conforms to the range of  $F$  values recommended by Ref. [47].

Table 2 lists the results of this analysis for the two water samples. Fisher and Spa have indeed a non-zero level of impurity (as indicated in “Results for the pure HPLC water sample and for the natural mineral water sample” section). No real system is ever entirely free of impurities; thus it is to be expected, but the values are low. In fact, even if the sample would be completely free of any other chemical compounds, the presence of surface melting and grain boundaries would still lead to some broadening. For the Fisher water a nominal impurity level of 5 ppm is given by the supplier, in reasonable agreement with the value obtained from the thermal data. These numbers show also that the Spa mineral water is nearly as pure as the Fisher water. On the bottle, the amount of impurities present can

**Table 2** Purity results for the two water samples

#	Name	$x_2$		
		van ’t Hoff ppm	ASTM ppm	M&D ppm
1	Fisher	11	19	22
2	Spa	17	22	24

$x_2$  is the molar concentration in Eq. (8), as determined from the analysis of the thermal data

actually be found, and this corresponds to an impurity level of 16 ppm, in good agreement with the number obtained from the thermal properties.

There is also a significant difference in the results between the linear van 't Hoff method on the one hand and the ASTM and M&D method on the other hand. This is caused by the fact that the linear approximation to the  $T(F^{-1})$  data is insufficient. It should be noted that this deficiency cannot be remedied by using the full van 't Hoff equation instead of the linearised form of Eq. (8). The similarity between the ASTM and M&D values can be expected when comparing the form of the relations: both use a modified form of  $F$ , with  $\epsilon$  or  $K$ , respectively, as a parameter. From a numerical point of view, these are nearly identical, and this is reflected by the similar results. This correspondence is all the more remarkable because in the case of the ASTM method; the data are fitted over the range from  $F = 0.1$  to  $F = 0.5$ , whereas for the M&D method, only three data points are considered.

## Summary and conclusions

In summary, we have used Peltier-element-based adiabatic scanning calorimetry (pASC) to revisit the phase diagram of water–NaCl from 0% to the eutectic concentration at 23.3% and between  $-30$  and  $5$  °C and to study the thermal properties. A series of samples were carefully heated to determine their equilibrium enthalpy  $h$  and heat capacity  $c_p$  during the melting process from a solid phase in which pure water ice and NaCl·2H<sub>2</sub>O are mixed, through a broad two-phase region consisting of a diminishing ice fraction in a salt solution, and finally into a homogenous liquid phase. These equilibrium enthalpy and heat capacity data were analysed to obtain the transition temperatures, transition enthalpies and the purity of the purest samples.

For this analysis to proceed, an advanced method for the calculation of the molten fraction  $F$  is applied, which is modified for the specific circumstances of a phase diagram with a eutectic transition. The innovation is to consider the two transitions, melting and eutectic, as parts of a single transition from solid to liquid with a wide two-phase region in between.

On the basis of the curve for  $F$ , the heats of fusion for the transition can be determined. The heat of fusion for the ice melting decreases with concentration, while it increases for the eutectic transition; the total transition heat, however, also decreases with concentration. After a rescaling for the amounts of the two fractions present in the two-phase region, it is seen that the heat of fusion for the eutectic fraction is constant as a function of concentration at  $235 \text{ J g}^{-1}$ . For the ice melting transition, the transition

heat data are close to the value for pure water, but decrease slightly with increasing concentration of salt.

In conclusion, we have demonstrated the usefulness of a high-resolution equilibrium calorimetric technique for a well-known phase diagram, confirming the transition temperatures. Additionally, the interpretation of the melting and eutectic transitions as being part of a single melting process allowed to improve the quality of the determination of the heats of fusion for these two transitions.

**Acknowledgements** This research was supported by the Research Foundation–Flanders (FWO) through research Project G.0492.10 “Nanoparticles in suspension: study of thermophysical behaviour by photothermal and related techniques” and by the Research Council of KU Leuven through research Project OT/11/064 “Investigation of exotic thermal and elastic behaviour of soft matter and functional thin layers by means of advanced experimental techniques”.

## References

- Pitzer KS, Peiper JC, Busey RH. Thermodynamic properties of aqueous sodium chloride solutions. *J Phys Chem Ref Data*. 1984;13(1):1–102. doi:10.1063/1.555709.
- Archer DG. Thermodynamic properties of the NaCl+H<sub>2</sub>O system. II. Thermodynamic properties of NaCl(aq), NaCl·2H<sub>2</sub>O(cr), and phase equilibria. *J Phys Chem Ref Data*. 1992;21(4):793. doi:10.1063/1.555915.
- Akinfiev NN, Mironenko MV, Grant SA. Thermodynamic properties of NaCl solutions at subzero temperatures. *J Solut Chem*. 2001;30(12):1065–80. doi:10.1023/A:1014445917207.
- Sedlbauer J, Wood RH. Thermodynamic properties of dilute NaCl(aq) solutions near the critical point of water. *J Phys Chem B*. 2004;108(31):11838–49. doi:10.1021/jp036775m.
- Driesner T, Heinrich CA. The system H<sub>2</sub>O–NaCl. Part I: correlation formulae for phase relations in temperature–pressure–composition space from 0 to 1000 °C, 0 to 5000 bar, and 0 to 1  $x_{\text{NaCl}}$ . *Geochim Cosmochim Acta*. 2007;71(20):4880–901. doi:10.1016/j.gca.2006.01.033.
- Driesner T. The system H<sub>2</sub>O–NaCl. Part II: correlations for molar volume, enthalpy, and isobaric heat capacity from 0 to 1000 °C, 0 to 5000 bar, and 0 to 1  $x_{\text{NaCl}}$ . *Geochim Cosmochim Acta*. 2007;71(20):4902–19. doi:10.1016/j.gca.2007.05.026.
- Fuentevilla DA, Sengers JV, Anisimov MA. Critical locus of aqueous solutions of sodium chloride revisited. *Int J Thermophys*. 2012;33(6):943–58. doi:10.1007/s10765-012-1201-5.
- Han B, Bischof JC. Thermodynamic nonequilibrium phase change behavior and thermal properties of biological solutions for cryobiology applications. *J Biomech Eng*. 2004;126(2):196–203. doi:10.1115/1.1688778.
- Han B, Choi JH, Dantzig JA, Bischof JC. A quantitative analysis on latent heat of an aqueous binary mixture. *Cryobiology*. 2006;52(1):146–51. doi:10.1016/j.cryobiol.2005.09.007.
- Thurmond VL, Brass GW. Activity and osmotic coefficients of sodium chloride in concentrated solutions from 0 to  $-40$ °C. *J Chem Eng Data*. 1988;33(4):411–4. doi:10.1021/je00054a007.
- Archer DG, Carter RW. Thermodynamic properties of the NaCl + H<sub>2</sub>O system. 4. Heat capacities of H<sub>2</sub>O and NaCl(aq) in cold-stable and supercooled states. *J Phys Chem B*. 2000;104(35):8563–84. doi:10.1021/jp0003914.
- Thoen J. Thermal investigations of phase transitions in thermotropic liquid crystals. *Int J Mod Phys B*. 1995;9(18–19):2157–218. doi:10.1142/S0217979295000860.

13. Leys J, Losada-Pérez P, Glorieux C, Thoen J. Application of a novel type of adiabatic scanning calorimeter for high-resolution thermal data near the melting point of gallium. *J Therm Anal Calorim.* 2014;177(1):173–87. doi:10.1007/s10973-014-3654-1.
14. Thoen J, Bloemen E, Van Dael W. Heat capacity of the binary liquid system triethylamine–water near the critical solution point. *J Chem Phys.* 1978;68(2):735–44. doi:10.1063/1.435746.
15. Bloemen E, Thoen J, Van Dael W. The specific heat anomaly in triethylamine–heavy water near the critical solution point. *J Chem Phys.* 1980;73(9):4628–35. doi:10.1063/1.440702.
16. Bloemen E, Thoen J, Van Dael W. The specific heat anomaly in some ternary liquid mixtures near a critical solution point. *J Chem Phys.* 1981;75(3):1488–95. doi:10.1063/1.442155.
17. Thoen J, Bloemen E, Marynissen H, Van Dael W. High-resolution calorimetric investigation of phase transitions in liquids. In: Proceedings of the 8th symposium on thermophysical properties. New York: Am. Soc. Mech. Eng. (ASME); 1982, pp. 422–429.
18. Thoen J, Marynissen H, Van Dael W. Temperature dependence of the enthalpy and the heat capacity of the liquid-crystal octyl-cyanobiphenyl (8CB). *Phys Rev A.* 1982;26(5):2886–905. doi:10.1103/PhysRevA.26.2886.
19. Thoen J, Marynissen H, Van Dael W. Nematic-smectic-A tricritical point in alkylcyanobiphenyl liquid crystals. *Phys Rev Lett.* 1984;52(3):204–7. doi:10.1103/PhysRevLett.52.204.
20. Thoen J, Cordoyiannis G, Glorieux C. Investigations of phase transitions in liquid crystals by means of adiabatic scanning calorimetry. *Liq Cryst.* 2009;36(6–7):669–84. doi:10.1080/02678290902755564.
21. Thoen J. High resolution adiabatic scanning calorimetry and heat capacities. In: Wilhelm E, Letcher TM, editors. Heat capacities: liquids, solutions and vapours. London: The Royal Society of Chemistry; 2010, pp. 287–306. doi:10.1039/9781847559791-00287.
22. Contreras-Gallegos E, Domínguez-Pacheco FA, Hernández-Aguilar C, Salazar-Montoya JA, Ramos-Ramírez EG, Cruz-Orea A. Specific heat of vegetable oils as a function of temperature obtained by adiabatic scanning calorimetry. *J Therm Anal Calorim.* 2017;128(1):523–31. doi:10.1007/s10973-016-5864-1.
23. Thoen J, Leys J, Glorieux C. Adiabatic scanning calorimeter, European patent: EP 2 591328 B1 (Sept. 02, 2015), US patent: US 9.310.263 B2 (April 12, 2016).
24. Leys J, Losada-Pérez P, Slenders E, Glorieux C, Thoen J. Investigation of the melting behavior of the reference materials biphenyl and phenyl salicylate by a new type adiabatic scanning calorimeter. *Thermochim Acta.* 2014;582:68–76. doi:10.1016/j.tca.2014.02.023.
25. Leys J, Glorieux C, Thoen J. Temperature dependence of enthalpy and heat capacity of alkanes and related phase change materials (PCMs) with a peltier-element-based adiabatic scanning calorimeter. *MRS Adv.* 2016;1(60):3935–40. doi:10.1557/adv.2016.298.
26. Leys J, Duponchel B, Longuemart S, Glorieux C, Thoen J. A new calorimetric technique for phase change materials and its application to alkane-based PCMs. *Mater Renew Sustain Energy.* 2016;5:4. doi:10.1007/s40243-016-0068-y.
27. Lide DR, editor. CRC handbook of chemistry and physics. 8th ed. Boca Raton: CRC Press; 2005.
28. Boudouh I, Hafsaoui SL, Mahmoud R, Barkat D. Measurement and prediction of solid–liquid phase equilibria for systems containing biphenyl in binary solution with long-chain *n*-alkanes. *J Therm Anal Calorim.* 2016;125(2):793–801. doi:10.1007/s10973-016-5407-9.
29. Egenolf-Jonkmanns B, Graen-Heedfeld J, Bruzzano S. Development of calorimetric methods for the characterization of different aqueous deicers. *J Therm Anal Calorim.* 2017;127(1):857–62. doi:10.1007/s10973-016-5426-6.
30. Gray DE, editor. American institute of physics handbook. 3rd ed. New York: McGraw-Hill; 1972.
31. Inaba H, Saitou T, Tozaki Ki. Effect of the magnetic field on the melting transition of H<sub>2</sub>O and D<sub>2</sub>O measured by a high resolution and supersensitive differential scanning calorimeter. *J Appl Phys.* 2004;96(11):6127–32. doi:10.1063/1.1803922.
32. Chen N, Morikawa J, Hashimoto T. Effect of cryoprotectants on eutectics of NaCl · 2H<sub>2</sub>O/ice and KCl/ice studied by temperature wave analysis and differential scanning calorimetry. *Thermochim Acta.* 2005;431(1–2):106–12. doi:10.1016/j.tca.2005.01.050.
33. Höhne GWH, Hemminger WF, Flammersheim HJ. Differential scanning calorimetry—an introduction for practitioners. Berlin: Springer; 1996. doi:10.1007/978-3-662-03302-9.
34. Atkins P. Physical chemistry. 6th ed. Oxford: Oxford University Press; 1998.
35. Kumano H, Asaoka T, Saito A, Okawa S. Study on latent heat of fusion of ice in aqueous solutions. *Int J Refrig.* 2007;30(2):267–73. doi:10.1016/j.ijrefrig.2006.07.008.
36. Pilcher G. A simplified calorimeter for the precise determination of purity. *Anal Chim Acta.* 1957;17:144–60. doi:10.1016/S0003-2670(00)87007-5.
37. Smit WM. Zusammenfassender Bericht. Purity determination by thermal analysis. *Z Elektrochem Ber Bunsenges Phys Chem.* 1962;66(10):779–87. doi:10.1002/bbpc.19620661005.
38. Blaine R, Schoff CK, editors. Purity determination by thermal analysis, special technical publication, vol. 838. West Conshohocken: Am Soc Test Mat (ASTM); 1984.
39. Plato C, Glasgow AR Jr. Differential scanning calorimetry as a general method for determining the purity and heat of fusion of high-purity organic chemicals. Application to 95 compounds. *Anal Chem.* 1969;41(2):330–6. doi:10.1021/ac60271a041.
40. Marti EE. Purity determination by differential scanning calorimetry. *Thermochim Acta.* 1972;5(2):173–220. doi:10.1016/0040-6031(72)85022-6.
41. Brown ME. Determination of purity by differential scanning calorimetry (DSC). *J Chem Educ.* 1979;56(5):310–3. doi:10.1021/ed056p310.
42. van Dooren A, Müller BW. Purity determinations of drugs with differential scanning calorimetry (DSC)—a critical review. *Int J Pharm.* 1984;20(3):217–33. doi:10.1016/0378-5173(84)90170-4.
43. Wunderlich B. Thermal analysis. New York: Academic; 1990.
44. Giron D, Goldbronn C. Place of DSC purity analysis in pharmaceutical development. *J Therm Anal Calorim.* 1995;44(1):217–51. doi:10.1007/BF02547150.
45. Rossini FD. Chemical thermodynamics. New York: Wiley; 1950.
46. Hamer WJ, Wu YC. Osmotic coefficients and mean activity coefficients of uni-univalent electrolytes in water at 25 °C. *J Phys Chem Ref Data.* 1972;1(4):1047–100. doi:10.1063/1.3253108.
47. ASTM. E928-08 standard test method for determination of purity by differential scanning calorimetry. doi:10.1520/E0928-08.
48. Mastrangelo SVR, Dornte RW. Solid solutions treatment of calorimetric purity data. *J Am Chem Soc.* 1955;77(23):6200–1. doi:10.1021/ja01628a037.